Two-Stage Optimal Design of Metro Underframe Structures: Based on Topology-Size-Shape Co-Optimization Methodology

Delei Du – Yana Li – Jian Song – Zhengping He – Jianxin Xu ✉
Key Laboratory of Railway Industry on Safety Service Key Technologies for High-speed Train, CRRC College, Dalian Jiaotong University, China
✉ xujianxinxjx@163.com

Abstract *The design of the metro body structure must balance both safety and cost indicators. The underframe is not only the main load-bearing component of the metro body but also accounts a significant portion of its overall mass. To reduce operational costs and enhance the safety performance of the metro body, this paper focuses on optimizing the design of the underframe. A two-stage optimization approach was proposed, addressing the limitation of existing methods and the challenges in balancing realistic operating conditions with manufacturability. First, manufacturing constraints were incorporated using the variable density method, and topology optimization of the underframe sub-model was carried out with the objective of minimizing flexibility-weighted strain energy. Next, the rough topology was refined through parametric optimization after determining the approximate shape of the cross section, resulting in a more precise model. The results show that the proposed optimization method reduces underframe mass by about 4.7 % while lowering the maximum deflection of the metro car body under the maximum vertical load case by 0.601 mm. This demonstrates that the proposed framework efficiently combines optimization capabilities with simplicity.*

Keywords *underframe, structural optimization, collaborative optimization, lightweighting*

Highlights
- *Joint topology, size and shape were optimized for reducing performance errors in reconfigured shapes.*
- *Multi-case weighting strategy simplified the calculation for varied engineering conditions.*
- *Improvement of vertical load form, closer to the actual environment, increasing the reliability of optimization.*
- *The mass of the underframe was reduced by 4.7 %, and the maximum vertical displacement was reduced by 0.601 mm.*

1 INTRODUCTION

Structural optimization design is an important part of the design process of locomotive body. Based on the form the of optimization, it can be clasified into topology optimization, size optimization, and shape optimization [1]. The rapid development of computers has created favorable conditions for the progress of optimal design, and the theory itself has become increasingly mature and widely applied in engineering practice [2-4]. Among these methods, topology optimization focuses on determining the optimal material distribution within a given design domain [5]. As a powerfull tool for the initial stage of structural design, topology optimization identifies topological configurations that represent the main transmission paths of physical information within the structure. This enables engineers to analyze how different shapes influence physical fields by interpreting these results [6-8]. In recent years, the research on topology optimization has intensified. Bai et al. [9] obtained hollow structures by the moving deformable component method, and achieved the first explicit 3D topology optimization for hollow structures by combining the internal and external topological description functions. Later, multi-material topology optimization was achieved by describing coating material distibution with multiple level set functions [10]. Similary, Guo et al. [11] combined the advantages of explicit and implicit topology optimization to introduce a new method for multi-material applications. Although these developmens mark significant progress, topology optimization still faces challenges that limit its full implementation in engineering practice.

Size optimization, as a parametric optimization tool, treats material dimensions as design variables [12]. Shape optimization, on the other hand, allows for small modifications to an existing structure to further exploit its mechanical performance [13,14]. Both size and shape optimization serve as structural refinement optimization tools that fine-tune dimensions and geometric details, thereby complementing the challenges of directly appling topology optimization results in engineering [15,16]. In recent years, researchers have increasingly combined these three optimization methods to form a two- or three-stage optimization frameworks, which have proven effective in numerous cases. For example, Tomás and Marti [17] applied shape optimization combined with size optimization in the design of a concrete shell, confirming the value of refinement optimization. Zhu et al. [18] utilized topology and size optimization for lightweight wind turbine blades design, achieving a 3 % reduction in mass. Wang et al. [19] combined topology optimization with shape optimization to develop an optimization algorithm for spatial steel frames with adaptable cross-section structures. Similarly, Zhao et al. [20] proposed a topology and size optimization strategy considering displacement, stress and stability constraints.

However, a single optimization method often cannot support engineers in designing structures that meet engineering realities while coping with complex environments. For this reason, researchers have approached the problem in two main ways. On the one hand, optimization algorithms have been refined to address specific requirements [21-23]. On the other hand, improving a particular algorithm is not always universally accepted, as its applicability may be limited. Therefore, some researchers changed the method the way optimization models impose working conditions to make the results more practical and reliaible. Bai et al. [24] investigated the three-point bending characteristics of a double rectangular thin-walled tube and analyzed its crashworthiness by equating the energy characteristics under those conditions. Sha et al. [25] proposed a multi-case topology

DOI: 10.5545/sv-jme.2025.1308

optimization method adapted for robots, enabling lightweight design while accounting for changes in robot posture. Golubin [26] derived a first-order necessary condition for optimal solutions based on geometrically preferred conical dyads, providng a reliable scheme for resolving optimization conflicts in structures subject to different working conditions. Zhu et al. [27] transformed the homogeneous load condition of the locomotive underframe into an equivalent centralized load condition. This approach solved the common problem in topology optimization where low strain energy leads to missing material in the middle region of the underframe.

Although structural optimization methods have been studied in depth, optimization of railroad locomotives has mainly focused on dimensions [28], materials [29] or individual components [30]. However, optimizing the entire locomotive body still presents challenges in practical application [31,32]. In this context, this paper proposes a two-stage optimization method to improve the structural performance of subway car bodies. In this paper, topology optimization serves mainly as a structural reshaping tool, while size and shape optimization act as refinement tools. The optimization strategy unfolds sequentially across two main stages. In the initial stage, topology optimization performed using a variable density approach with manufacturing constraints, targeting the minimization of flexibility-weighted strain energy. This process yields an initial material layout. In the second stage, this layout is refined through parametric optimization, combining dimensional optimization (to adjust plate thickness) and shape optimization (to refine the geometry of corrugated plate nodes). This synergistic approach ensures the attainment of high-performance structural solutions without compromising manufacturability. In the topology optimization stage, 3D optimization is superior to 2D optimization in terms of material distribution [3]. Therefore, the chassis model was discretized into solid elements, and a multiple-case equally weighted compromise planning method is used to simsplify the multi-objective function problem into a single-objective function problem [33]. The model is then reconstructed according to the topology results, with the upper and lower bounds for size optimization defined by sensitivity values. Finally, the cross-sectional shapes are refiened through shape optimization. To better simulate actual engineering conditions, vertical loads are applied incrementally as step loads toward the middle section before size optimization. The results show that this form of optimization method effectively reduces reconstruction error from topology results and produces a more accurate cross-section layout of the underframe.

2 METHODS AND MATERIALS

2.1 Topology Optimization

Topology optimization determines the optimal material distribution that maximizes structural stiffness. Based on the material distribution cloud diagram from the topology result, the main force transmission path of the underframe can be determined, which in turn provides guidance for the preliminary layout of the corrugated plate. To further quantify the influence of the material properties on structural stiffness, it is necessary to establish the relationship between the material's elastic modulus and its density. This relationship can be expressed as a functional dependence of the elastic modulus on the density:

$$E(\rho_e) = E_{\min} + \rho_e^p (E_0 - E_{\min}), \quad \rho_e \in [0,1]. \tag{1}$$

In Equation (1), ρ_e represents the relative density of the material, which serves as thedesign variable in topology optimization. E_0 is the elastic modulus of the original material, while $E_{\min}$ is the elastic modulus to elements that are effectively removed during optimization. The parameter p denotes the penalty coefficient within solid isotropic material with penalization (SIMP) algorithm, which controls the material removal rate, defined as $p \in (1,5]$. Generally, larger values of p enhance the suppression of intermediate densities, which makes the material distribution closer to a clear 0-1 (void-solid) state. However, excessively high penalty values can substantially increase the burden of computation.Therefore, in practical engineering applications, $p=3$ is most commonly adopted [5].

In multi-stiffness optimization, the optimal topology varies across different working conditions. Since real engineering applications must withstand multiple load conditions, combining these conditions yields results that are more representative of practical performance. In this paper, we establish a mathematical model for multi-stiffness topology optimization and implement it in OptiStruct using a custom function. By applying the compromise planning method, the multi-objective problem is transformed into a single-objective problem, enabling a balanced and computationally efficient solution.

$$C(\rho) = \left[\sum_{k=1}^{m} \omega_k^p \left(\frac{C_k(\rho) - C_k^{\min}}{C_k^{\max} - C_k^{\min}} \right)^p \right]^{\frac{1}{p}}. \tag{2}$$

In Equation (2), ρ is the design variable, $C(\rho)$ objective function defined by compliance, m total number of conditions, ω_k weighted compliance value of the k^{th} working condition. Since stiffness maximization is typically equivalent to the compliance minimization, this formulation is standard in structural optimization. Notation p is the penalty coefficient, and $C_k(\rho)$ represent a compliance function, and $C_k^{\max}$ and $C_k^{\min}$ are the maximum and minimum values, respectively.

In addition, minimum and maximum member size constraints are considered in the optimization process to prevent occurrence of free cells and excesive material accumulation. The minimum member size constraint is enforced through the density filtering function, ensuring that structural features remain manufacturable and mechanically meaningful.

$$\tilde{\rho}_i = \frac{\sum_{j \in \Omega(i)} \omega_{ij} \rho_j}{\sum_{j \in \Omega(i)} \omega_{ij}}, \quad \omega_{ij} = \max\left(0, r_{\min} - \left\| \mathbf{x}_i - \mathbf{x}_j \right\|\right), \tag{3}$$

where $\tilde{\rho}_i$ is the filtered design variable, ρ_j original material density, ω_k weight coefficient, and $\Omega(i)$ neighborhood centered on cell i with radius r, where $r_{\min}$ coresponds to the minimum member size radius.

The maximum member size constraint is enforced using inverse density filtering, ensuring that overly large structural members do not form during the optimization process.

$$\tilde{\rho}_e = 1 - \frac{\sum_{i \in \Omega(i)} \omega_{ij} (1 - \rho_j)}{\sum_{i \in \Omega(i)} \omega_{ij}}, \quad \Omega(i) = \left\{ j \mid \left\| \mathbf{x}_j - \mathbf{x}_e \right\| \le r_{\max} \right\}. \tag{4}$$

At this point $r_{\max}$ is the maximum size radius. In summary, the mathematical model for the subway underframe section based on the compromise planning method can be expressed as follows:

find: $\rho = (\rho_1, \rho_2, \ldots, \rho_n)^T$,

$$\min: C(\rho) = \left[\sum_{k=1}^{m} \omega_k^p \left(\frac{C_k(\rho) - C_k^{\min}}{C_k^{\max} - C_k^{\min}} \right)^p \right]^{\frac{1}{p}},$$

$$\text{s.t.}: \sum_{k=1}^{m} \left(\sum_{j=1}^{n} V_j \rho_j^k \right) - V_z \le 0,$$

$$\tilde{\rho}_i = \frac{\sum_{j \in \Omega(i)} \omega_{ij} \rho_j}{\sum_{j \in \Omega(i)} \omega_{ij}}, \quad \tilde{\rho}_e = 1 - \frac{\sum_{i \in \Omega(i)} \omega_{ij} (1 - \rho_j)}{\sum_{i \in \Omega(i)} \omega_{ij}},$$

$$0 < \rho_{\min} \le \rho_j < 1, \quad j = 1, 2, \ldots, n, \quad k = 1, 2, \ldots, m.$$

In the above formula, V_j is volume of the j^{th} cell, V_z maximum volume in the design space of the model, and s.t. the constraint", while n is a total number of units in the design domain. In this paper, the volume fraction was used as the constraint.

2.2 Plate Thickness Size Optimization

Sensitivity analysis is an analytical method used to investigate how sensitive a system's response is to changes in model parameters, arising either from variations in operating states or from internal modification of the model itself. The response sensitivity with respect to a design variable can be expressed as follows:

$$[\mathbf{K}]\{\mathbf{U}\}=\{\mathbf{P}\}. \tag{5}$$

Taking partial derivatives on both sides of the above equation, respectively.

$$\frac{\partial[\mathbf{K}]}{\partial x_i}\{\mathbf{U}\}+[\mathbf{K}]\frac{\partial\{\mathbf{U}\}}{\partial x_i}=\frac{\partial\{\mathbf{P}\}}{\partial x_i}. \tag{6}$$

Vector **U** partial derivatives:

$$\frac{\partial\{\mathbf{U}\}}{\partial x_i}=[K]^{-1}\left(\frac{\partial\{\mathbf{P}\}}{\partial x_i}-\frac{\partial[\mathbf{K}]}{\partial x_i}\{\mathbf{U}\}\right). \tag{7}$$

In Equation (7), $\partial\{\mathbf{U}\}/\partial x_i$ represents the sensitivity of the objective function with respect to the design variable x_i. In this paper, the traditional approach to sensitivity analysis is adopted, while also considering the setting of constraint objectives during size optimization. Accordingly, both displacement sensitivity and mass sensitivity are selected as the primary reference sensitivity values in the analysis.

Based on the determined layout of the corrugated plate cross-section, the chassis section was further refined by optimizing the cross-sectional area of the reinforcing plate. Bending resistance is one of the key criteria for evaluating vehicle structural performance; therefore displacement parameters of the model are considered in the optimization process of this paper. The specific optimization model is formulated as follows:

find: $X=\{x_1,x_2,\ldots,x_{15}\}$,

min: $U_{size}=\min\mathbf{u}(d)$,

s.t.: $x_{\min}\le x_i\le x_{\max}$,

$\sigma_{\max}-90\text{ MPa}\le 0$,

$\sum_{i=1}^{n} mass_{xi}-1.1mass_z\le 0$,

where X is the design variable, U_{size} maximum displacement of the model node, $\mathbf{u}(d)$ displacement vector, $x_{\min}$, $x_{\max}$ upper and lower limits of the thickness of the reinforcing plate, $\sigma_{\max}$ maximum stress under the constraints of the model, $mass_{xi}$ mass of the i^{th} design variable, and $mass_z$ mass of the current structural model.

It was worth noting that, according to the EN 12663:2010 standard [34], the factor of safety for the yield strength of the body material must exceed 1.5. However, since this study focuses specifically on the underframe, more conservative stress constraints as well as higher mass redundancy are adopted. Section 2.3 adheres to the same constraint rules for constraints, maintaining consistency across the design process.

2.3 Shape Optimization

Shape optimization integrates geometric modeling, structural analysis and optimization [35]. It is an optimization design technique that refines structural boundaries or shapes by adjusting the node positions of the finite element model. Once the underframe cross-section structure is determinded, shape optimization can be applied to make localized structural distribution adjustments of the corrugated reinforcing plate. These refinements enhace the structural stiffness or strength while ensuring compliance with the principle of stiffness coordination. The specific optimization model is defined as follows:

find: $S=(s_1,s_2,\ldots,s_{28})^T$,

min: $U_{shape}=\min\mathbf{r}(d)$,

s.t.: $S_m\le S_i\le S_l$,

$\sigma_{\max}-60\text{ MPa}\le 0$,

$\sum_{i=1}^{n} mass_{xi}-1.1mass_{z1}\le 0$,

where S is the design variable representing shape optimization control displacement matrix, U_{shape} maximum displacement of the model node, $\mathbf{r}(d)$ displacement vector, S_m, S_l upper and lower limits of the node displacement of the reinforcing plate, $\sigma_{\max}$ maximum stress under the constraints of the model, and $mass_{xi}$ mass of the i^{th} design variable. $mass_{z1}$ is the mass of the current structural model.

2.4 Subway Underframe Section Status

The research object of this paper was the head section of a specific subway model, focusing on the original underframe cross-section structure, as shown in Fig. 1c. The body structure consist of large cross-section aluminum profiles combined with plate welding, while the underframe is made of aluminum alloy 6005A-T6. The 6000-series aluminum alloys are known for their excellent bending performance and are widely applied in the manufacturing of complex extruded parts. After finite element simplification, the main dimensions of the chassis were defined as follows: excluding the side beams, the transverse width of the chassis is 2500 mm, five corrugated plates are overlapped, each with a thickness of 2.5 mm, and the surface plate thickness is 2.8 mm.

Passengers in a train are in direct contact with the floor, which was subjected to vertical loads.The bending stiffness of the underframe is therefore a key criterion for evaluating the safety of the locomotive. During the process of structural optimization, the maximum displacement of the model can seve as a reference parameter, or it can be defined directly as both a target and a constraint condition.

In the optimization process, the boundary conditions can be defined with reference to the operating conditions of the metro body. In this paper, the operating conditions of the metro were established in accordance with [34], taking into account the calculation standards and detailes outlined in Section 2.5.

2.5 Load Conditions

The cross-section of the selected metro underframe is a hollow aluminum alloy plate with a corrugated structure, divided into five overlapping segments. This configuration provides good ductility, low weight, and high impact resistance. To ensure that the simulated load conditions closely reflect actual engineering scenarios and to improve the accuracy of load path calculation, four static strength conditions were selected: maximum vertical load, longitudinal tensile load, longitudinal compressive load and torsion load .

Table 1. The reference load case of the subway

Conditions	Load case description	Load
LC01	Maintenance mass and maximum overload	$g\times(m_1+m_4)$
LC02	Compression condition	1200 kN
LC03	Tensile condition	960 kN
LC04	Torsional condition	40 kNm

g is gravitational acceleration; m_1 car body weight, and m_4 passenger mass in overloaded conditions

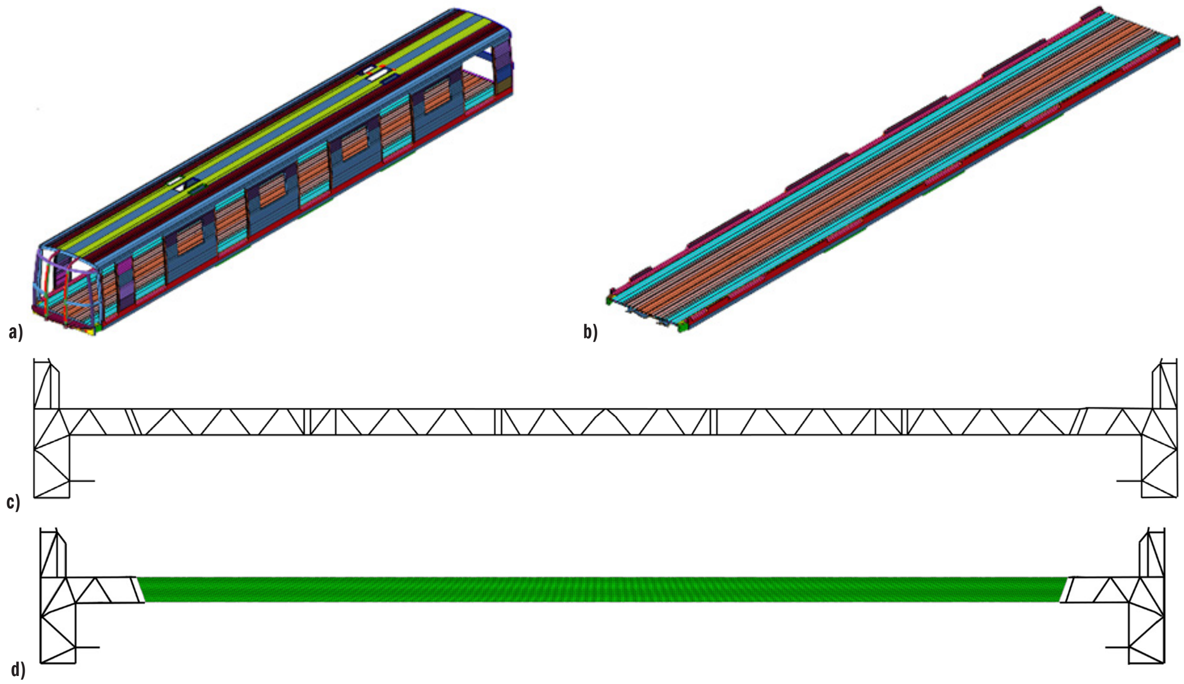

Fig. 1. Metro underframe structure and design domains; a) metro car body structure diagram, b) underframe structure diagram, c) underframe side beams, and d) underframe design domains

As presented in Fig. 1, the design domain represents the primary region for applying model loads. The constraints were imposed at the lap joints between the side beams and the bottom frame. From this design domain, the arrangement, shapes, and dimensions of the corrugated plates were developed and optimized. The corresponding optimization results and their analysis are presented in Section 3.

3 RESULTS AND DISCUSSION

The optimization process of the metro underframe cross-section was carried out in two stages. In the first stage, topology optimization was applied to reconfigure the layout of the cross-section corrugated plates. In the second stage, parameterized size optimization was performed to refine the corrugated plate thickness, while shape optimization was conducted by adjusting the relative position of the upper and lower nodes of the corrugated plates.

3.1 One Stage Topology Optimization and Result Analysis

Submodels were typically established by extracting submodel boundary moments or displacements under specific operating conditions, depending on the capabilities of the software [36,37]. However, in the case of metro bodies, the application is constrained by the length of the body. The submodel boundary conditions of the chassis section are only valid at the intercepted position in the chassis, which means that the resulting topological configuration cannot be directly applied to the entire vehicle [38].

Therefore, this paper establishes the model shown in Fig. 1d, setting the finite element model in the design domain as a solid element to better observe the force transfer path under loading. According to the topology optimization rules for the metro underframe, the volume of the topology configuration accounts for 0.3 of the design domain. At the same time, based on the compromise planning method, equal weighting was applied, with the maximum vertical load used as the primary working condition. Four groups of different forms of topological configurations with different forms were obtained. By summarizing these four groups of configurations, a resonstructed underframe section was derived to produce a rough new cross-sectional shape. The advantage of this approach is that it allows observation under different combinations of working conditions, highlighting the common force-bearing regions, while avoiding conflicts between conditions, e.g., combining tensile and compressive states.

According to the optimization rules described above, the iterations for four combined condition models converged within 54 to 67 steps. The corresponding material layout contours and the reconstructed model cross-section structure after convergence are shown in Fig. 2.

The topological cloud cross-section was roughly divided into three regions, A, B, and C, according to the material retention density, and the four topological clouds in Fig. 3 were summarized accordingly. Region A is located near the edge beams, experiancing the largest bending moments. As a result, the material retention density was generally higher. However, the boundaries of the material retention zones were diffuze, and reinforcing plates tendet to intersect. To avoid stress concentration, this region was reconstructed with a triangular reinforcing plate structure, connected at both ends. During verification of the rough model, high stress concentrations were observed at the edges, so an additional reinforcing plate was added in the middle of the section to meet this requirement. In region C, most of the material was removed, and a distinct topological configuration appeared only when torsional loading carried a greater weight. Since torsional loading is a frequent operational condition for the metro bodies, a reinforcing plate was added to be placed in the middle of the section to meet this requirements. Region B had a wider span with clearer topological configuration. The force transsmition paths were more consistent across all four combined loading conditions. However, reinforcing plates in certain locations had significant effect on stress and displacement. For simplification, the reiforcing plates in B region were reduced as shown in Fig. 3 above. Finally, considering manufacturability, the optimized underframe was divided into five spliced segments. The lap joints relied on two parallel reinforcing plates, with parallel edges at the overlap boundaries, as illustrated in Fig. 3.

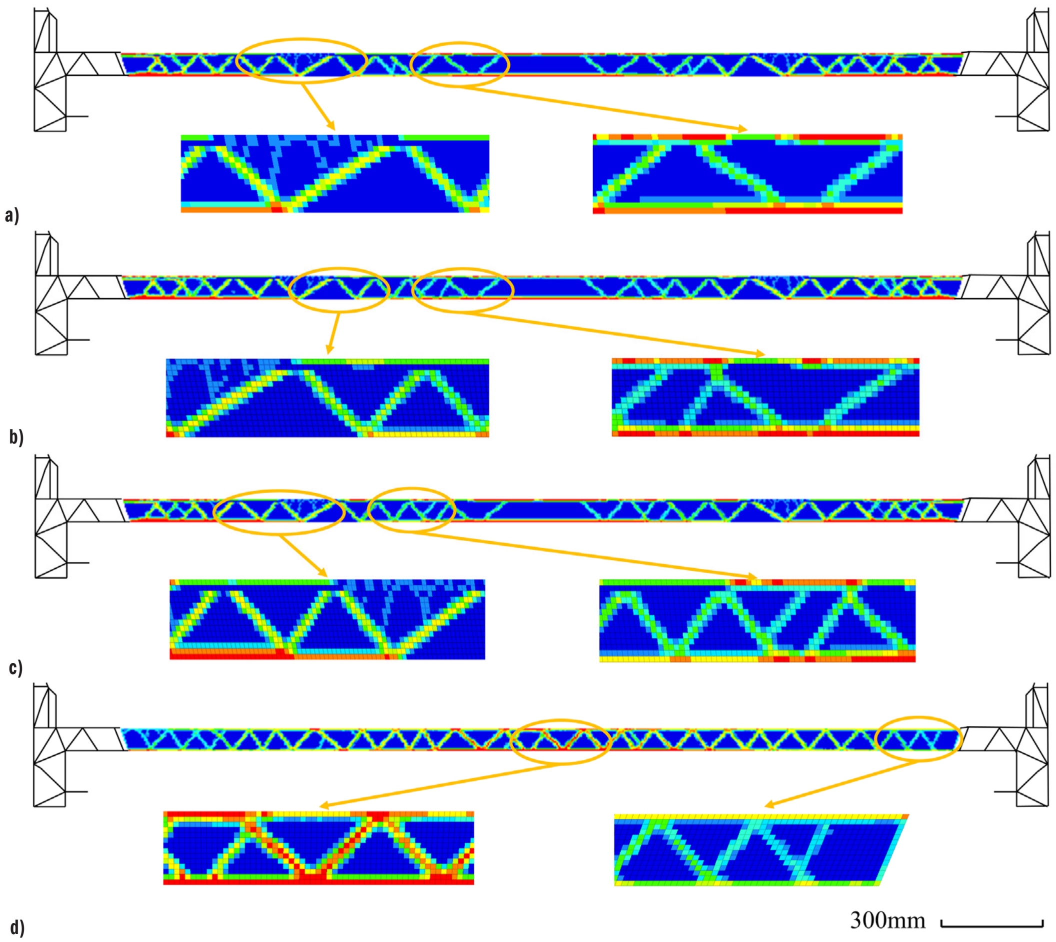

Fig. 2. Topological configuration and rough cross section structure ; a) maintenance mass and maximum overload & compression condition with 1200 kN; b) maintenance mass and maximum overload & tensile condition with 960 kN, c) maintenance mass and maximum overload & torsional condition, and d) maintenance mass and maximum overload & compression condition with 1200 kN

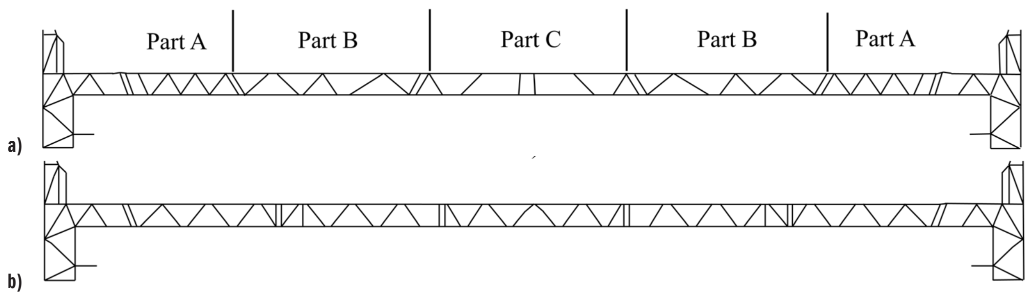

Fig. 3. Comparison of cross-section shapes of chassis; a) reconstructed section, and b) original section

3.2 Two Stage Size Optimization and Result Analysis

To comprehensively evaluate the impact of parameter changes on the models for each part of the design variables, relative sensitivity [39,40] was adopted in this paper as the basis for the design optimization scheme. Relative sensitivity is defined as the ratio of displacement sensitivity to mass sensitivity, enabling a more comprehensive assessment of design variable sensitivity.

The maximum synthetic displacement in the computational model was 2.991 mm, with the maximum displacement point located in the middle of the computational model. To analyze sensitivity to plate thickness, 9 nodes were extracted from the upper and lower surfaces of the longitudinal section passing through this point, The initial thickness of all plates was 2.5 mm. Finally, the calculated sensitivity data were weighted equally. Since metro underframes are tipically left-right symmetric structures, and the reinforcement plates follow the same symmety, only one side of the model was considered as a reference for optimization. On this side, 20 reinforcement plates were present. To reduce the computational workload while maintaining engineering relevance, these 20 reinforcing plates were categorized into 15 component combinations according to their stress conditions.

Based on the magnitude of the absolute sensitivity values, the degree to which Objective function 1 responds to changes in the design variables can be determined. Therefore, taking the absolute value of the sensitivity parameter of each component for comparison, the 15 design variables were categorized into four categories with similar sizes: The first category has a sensitivity range of 57 to 84. The design variable was limited to between 70 % of the initial plate thickness and a maximum of 3 mm. The second category has sensitivity range of 187 to 294. Compared with the first group, these design variables show much larger sensitivity changes. Therefore, their maximum plate thickness was increased from 5 mm to 6 mm. The third category falls within a sensitivity range of 436 to 656, which is significantly higher. For this group, the design variables were set to 70 % of the initial plate thickness and a maximum plate thickness of 8 mm. The fourth category shows the larger sensitivity ranging from 941 to 1066. Taking process requirements into account, the maximum thickness limit for this group of design variables was further expaned to 10 mm.

Considering the engineering reality, the vertical load of the underframe is complex. In this study, the distribution form of the maximum vertical load was modified, and the resulting optimization outcomes were sorted out using the mathematical expectation method. According to the sensitivity rules, the calculated dimensions are shown in Table 2, and the coresponding comparisons are ilustrated in Fig. 4.

Table 2. Design variable parameters

Variable class	Comp.	Opt. value 1 [mm]	Opt. value 2 [mm]	Opt. value 3 [mm]	Expect. sort. [mm]	Adj. value [mm]
First	S5	1.75	1.75	1.88	1.79	1.80
	S6	1.75	1.75	1.99	1.83	1.80
	S8	1.75	1.75	1.75	1.75	1.80
	S11	1.75	1.75	1.75	1.75	1.80
	S12	1.75	1.75	1.75	1.75	1.80
Second	S2	5.58	5.43	5.00	5.34	5.50
	S7	2.53	2.54	4.23	3.10	3.00
	S10	2.20	4.67	6.21	4.36	4.50
	S13	3.25	3.23	5.00	3.83	3.80
	S15	1.75	1.75	3.01	2.17	2.00
Third	S1	1.75	1.75	1.88	1.79	1.80
	S14	4.74	4.67	6.21	5.21	5.00
Fourth	S3	1.75	1.75	1.75	1.75	1.80
	S4	1.75	1.75	1.75	1.75	1.80
	S9	3.80	3.63	5.17	4.20	4.00

where Comp. stands for component, Opt. value for optimization value, Expect. sort. for expectation sorting and Adj. value for adjustment value

3.3 Two Stage Shape Optimization and Result Analysis

The shape optimization technique in OptiStruct allows manual definiton of deformation nodes to optimize the model geometry. As shown in Fig. 5, nodes were placed at the connection between the reinforcing plate and the upper and lower surfaces of the underframe, reflecting the actual engineering needs. A total of 28 points of interest were selected, where the deformation nodes were permitted to vary in the range of ±5 mm in the y-direction.

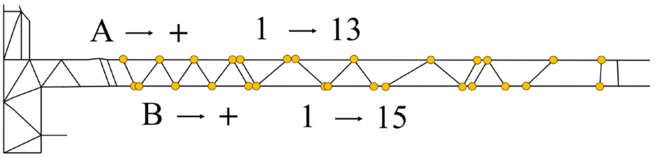

Fig. 5. Positive direction and deformation point serial number

The shape optimization was performed under the original vertical load condition, and an optimization model based on the control handle was established. After two optimization iterations, the deformation analysis showed that the displacement of the deformation point occures along the y-axis. The optimal solution was reached under the constraint that the deformation distance was limited to ±5 mm. Considering the manufacturing process requirements, the regularized displacement and direction of the deformation points are shown in Table 3.

Shape optimization is an effective approach to avoid local stress concentrations and achieve locally optimal solutions. As shown in Table 3, the displacement of each node was successfully controlled within ±5 mm. Among them, the symbols "+" and "–" denote the node displacement directions, and this asymmetric displacement pattern reflects the targeted adjustment of the load path. At the same time, it could be observed that the actual displacement of most nodes utilized only about 50 % of the allowable range, or even less. This indicate that, after completing the size optimization stage, the model had no obvious defects, but still retained potential for further improvement. This outcone verifies the effectiveness of shape optimization stage in enhancing local performance.

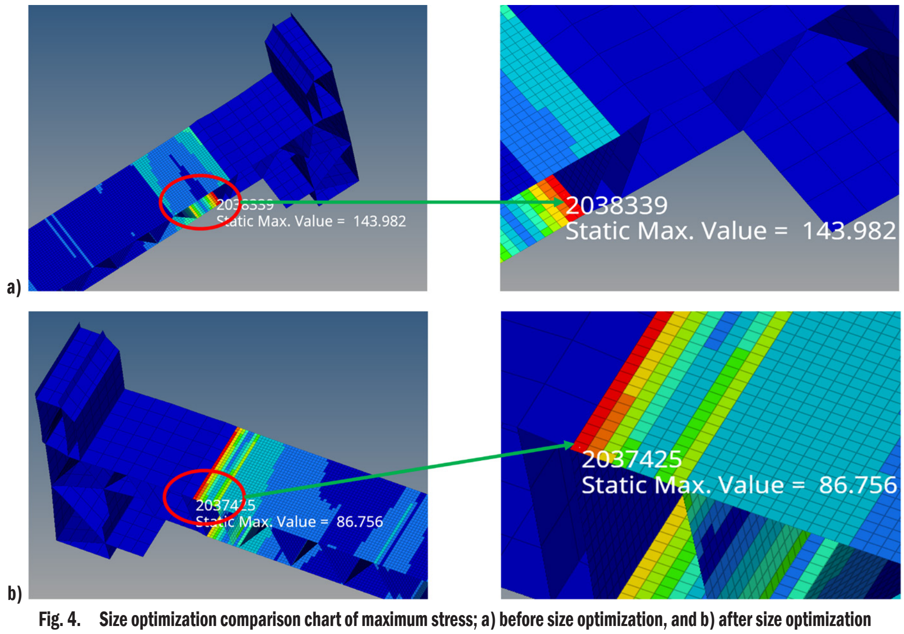

Fig. 4. Size optimization comparison chart of maximum stress; a) before size optimization, and b) after size optimization

Table 3. Graphical representation showing the displacement and direction of deformation points

Point (up)	Distance [mm]	Point (down)	Distance [mm]
A1	-2.6	B1	+1.8
A2	-2.2	B2	-1.7
A3	-2.3	B3	-2.5
A4	-2.3	B4	+2.6
A5	+2.3	B5	+2.4
A6	-1.7	B6	-2.5
A7	+2.1	B7	+1.3
A8	+2.3	B8	-1.3
A9	+2.5	B9	+1.9
A10	+2.5	B10	-2.1
A11	+2.3	B11	+2.6
A12	-2.0	B12	-2.4
A13	-2.3	B13	+2.0
		B14	-2.2
		B15	-2.6

3.4 Optimization Results Analysis

The optimized results are summarized in Table 4, which compares the key performance parameters of the subway car body before and after the two-stage optimization. The evaluation focuses on three indicators: mass, stress and maximum vertical displacement. After optimization, the mass was reduced from 7.354 tons to 7.170 tons, achieving a weight reduction of 0.184 tons, which significantly meets the lightweighting objective. The maximum stress increased only slightly, from 86.91 MPa to 87.12 MPa, a negligible change of 0.19 MPa. This value ramains far below the yield strength of 6005A-T6 aluminum alloy (≥ 215 MPa), thereby fully complying with the EN 12663 standard [34] requirement of a safety factor ≥1.5. At the same time, the maximum vertical displacement decreased from 22.691 mm to 22.090 mm, representing an improvement of 0.601 mm. These data fully verify the effectiveness of the proposed two-stage optimization method, which improves both structural lightweighting and performance enhancement while ensuring compliance with safety standards.

Table 4. Optimize the front and rear car body performance parameters

	Mass [t]	Stress [MPa]	Maximum vertical displacement [mm]
Front	7.354	86.91	22.691
Rear	7.17	87.12	22.090
Difference value	0.184	–0.19	0.601

4 CONCLUSION

This paper proposed a novel two-stage optimization method for the subway car body underframe, based on multiple operating conditions with a focus on both simplicity and efficiency. The optimized results achieved a correction of 0.601 mm for the maximum vertical displacement while satisfying all structural performances. Additionally, the mass of underframe was reduced by 0.184 t, (4.7 % of the mass of underframe). The following conclusions can be drawn from the research results:

a. Traditional single-optimization approaches are unsuitable for complex operating conditions, wheras the proposed method effectively overcomes this limitations.
b. The layout of the corrugated plate should account for stress concentration at the connection between the upper and lower underframes to ensure the stability and safety of the structure.
c. The introduction of multi-condition weighted strategies offers a practical and efficient solution to simplify computational complexity in multi-objective optimization.
d. The weight ratios of different working conditions significantly influence the optimization results, Therefore, adjusting these ratios can bring the outcomes closer to engineering reality, offering a promising direction for future research.

References

[1] Lee, H.J., Mancini, J.A., Joshipura, I., Spadaccini, C.M., Loh, K.J. Selective heating through Y-junction waveguide designed by acoustic shape optimization. *Adv Eng Mater* 25 2200756 (2023) **DOI:10.1002/adem.202200756**.

[2] Qin, L.Y., Yang, S.Y., Li, H.Z., Dai, J.C., Wang, G.S., Ling, Q.S., Chen, Z.W. Crashworthiness design of bionic-shell thin-walled tube under axial impact. *J Mech Sci Tec* 37 3427-3436 (2023) **DOI:10.1007/s12206-023-0608-1**.

[3] Liu, Z.J., Cho, S., Takezawa, A., Zhang, X.P., Kitamura, M. Two-stage layout-size optimization method for prow stiffeners. *Int J Nav Archit Ocean Eng* 11 44-51 (2019) **DOI:10.1016/j.ijnaoe.2018.01.001**.

[4] Cho, J.G., Koo, J.S., Jung, H.S. A lightweight design approach for an EMU carbody using a material selection method and size optimization. *J Mech Sci Tech* 30 673-681 (2016) **DOI:10.1007/s12206-016-0123-8**.

[5] Eschenauer, H.A., Olhoff, N. Topology optimization of continuum structures: A review. *Appl Mech Rev* 54 331-390 (2001) **DOI:10.1115/1.1388075**.

[6] Qi, L., Zhou, J.X., Jin, P.C., Wang, M.M., Su, Y.Z., Zhou, H.Y., Liu, G.C., Song, L.R. Low noise optimization of two-stage gearbox housing structure based on acoustic contribution analysis and topology optimization. *J Mech Sci Tech* 37 4533-4544 (2023) **DOI:10.1007/s12206-023-0810-1**.

[7] Tejani, G.G., Savsani, V.J., Patel, V.K., Savsani, P.V. Size, shape, and topology optimization of planar and space trusses using mutation-based improved metaheuristics. *J Comput Des Eng* 5 198-214 (2018) **DOI:10.1016/j.jcde.2017.10.001**.

[8] Yvonnet, J., Da, D. Topology optimization to fracture resistance: a review and recent developments. *Arch Comput Meth Eng* 31 2295-2315 (2024) **DOI:10.1007/s11831-023-10044-9**.

[9] Bai, J., Zuo, W. Hollow structural design in topology optimization via moving morphable component method. *Struct Multidisc Optim* 61 187-205 (2020) **DOI:10.1007/s00158-019-02353-0**.

[10] Bai, J., Zuo, W. Multi-material topology optimization of coated structures using level set method. *Compos Struct* 300 116074 (2022) **DOI:10.1016/j.compstruct.2022.116074**.

[11] Guo, Y., Liu, C., Guo, X. Shell-infill composite structure design based on a hybrid explicit- implicit topology optimization method. *Compos Struct* 337 118029 (2024) **DOI:10.1016/j.compstruct.2024. 118029**.

[12] Grihon, S., Krog, L., Bassir, D. Numerical optimization applied to structure sizing at AIRBUS: a multi-step process. *Int J Simul Multidisc Des Optim* 3 432-442 (2009) **DOI:10.1051/ijsmdo/2009020**.

[13] Gui, C., Bai, J., Zuo, W. Simplified crashworthiness method of automotive frame for conceptual design. *Thin Wall Struct* 131 324-335 (2018) **DOI:10.1016/j.tws.2018.07.005**.

[14] Bai, J., Li, Y., Zuo, W. Cross-sectional shape optimisation for thin-walled beam crashworthiness with stamping constraints using genetic algorithm. *Int J Vehicle Des* 73 (2017) **DOI:10.1504/IJVD.2017.082582**.

[15] Sekulski, Z. Least-weight topology and size optimization of high speed vehicle-passenger catamaran structure by genetic algorithm. *Mar Struct* 22 691-711 (2009) **DOI:10.1016/j.marstruc.2009.06. 003**.

[16] Bai, J., Zhao, Y., Meng, G., Zuo, W. Bridging topological results and thin-walled frame structures considering manufacturability. *J Mech Des* 143 091706 (2021) **DOI:10.1115/1.4050300**.

[17] Tomás, A., Martí, P. Shape and size optimisation of concrete shells. *Eng Struct* 32 1650-1658 (2010) **DOI:10.1016/j.engstruct.2010.02.013**.

[18] Zhu, J., Cai, X., Ma, D.F., Zhang, J.L., Ni, X.H. Improved structural design of wind turbine blade based on topology and size optimization. *Int J Low-Carbon Tech* 17 69-79 (2022) **DOI:10.1093/ijlct/ctab087**.

[19] Wang, C., Du, Z., Zhang, Z., Guo, X. Collaborative optimization of topology and cross-sectional shape for space frame structures. *Chin J Theor Appl Mech* 57 937-947 (2025) **DOI:10.6052/0459-1879-24-534**.

[20] Zhao, L., Li, Y., Cai, J., Yi, J., Zhou, Q., Rong, J. Integrated topology and size optimization for frame structures considering displacement, stress, and stability constraints. *Struct Multidisc Optim* 67 48 (2024) **DOI:10.1007/s00158-024-03766-2**.

[21] Körpe, D.S., Güzelbey, I.H. NACA four-digit airfoil series optimization: a comparison between genetic algorithm and sequential quadratic programming. *J Mech Sci Tech* 37 2375-2382 (2023) **DOI:10.1007/s12206-023-0414-9**.

[22] Garcia-Andrés, X., Gutiérrez-Gil, J., Martínez-Casas, J., Denia F.D. Wheel shape optimization approaches to reduce railway rolling noise. *Struct Multidisc Optim* 62 2555-2570 (2020) **DOI:10.1007/s00158-020-02700-6**.

[23] Hu, M.Z., Wang, H.X., Wei, P.T., Liu, G.S., Zhang, L., He, Z. Q., Liu, H.J. Multi-objective optimization of a co-rotating twin-screw gear transmission system based on heuristic search. *J Mech Sci Tech* 37 5831-5841 (2023) **DOI:10.1007/s12206-023-1022-4**.

[24] Bai, J., Meng, G., Wu, H., Zuo, W. Bending collapse of dual rectangle thin-walled tubes for conceptual design. *Thin Wall Struct* 135 185-195 (2019) **DOI:10.1016/j.tws.2018.11.014**.

[25] Sha, L.S., Lin, A.D., Xi, Q., Kuang, S.L. A topology optimization method for robot light-weight design under multi-working conditions and its application on upper-limb powered exoskeleton. *International Conference on Artificial Intelligence and Electromechanical Automation* 17-22 (2020) **DOI:10.1109/AIEA51086.2020.00011**.

[26] Golubin, A.Y. A Note on optimality conditions for multi-objective problems with a euclidean cone of preferences. *J Optim Theory Appl* 166 791-803 (2015) **DOI:10.1007/s10957-014-0698-0**.

[27] Zhu, Y., Liao, L., Ma, R., Yao, S. Research on collaborative optimization of high-speed train car body section profiles. *J Railway Sci Eng* (2025) **DOI:10.19713/j.cnki.43-1423/u.T20250747**.

[28] Liu, Y., Yang, B., Xiao, S. N., Zhu, T., Yang, G., Xiu, R. Parameter study and multi-objective optimization for crashworthiness of a B-type metro train. *P I Mech Eng F-J Rai* 236 91-108 (2022) **DOI:10.1177/ 09544097211008283**.

[29] Wang, J., Yang, B., Tian, H., Wang, W., Sang, X. Optimization design and mechanical performance study of carbon fiber-reinforced composite load-carrying structures for subway driver cabin. *Materials* 18 2524 (2025) **DOI:10.3390/ma18112524**.

[30] Guo, W., Xu, P., Yang, C., Guo, J., Yang, L., Yao, S. Machine learning-based crashworthiness optimization for the square cone energy-absorbing structure of the subway vehicle. *Struct Multidisc Optim* 66 182 (2023) **DOI:10.1007/s00158-023-03629-2**.

[31] Wang, D., Xu, P., Xiao, X., Kong, L., Che, Q., Yang, C. Multiobjective and multicollision scenario reliability-based design optimization of honeycomb-filled composite energy-absorbing structures for subways. *Struct Multidisc Optim* 65 238 (2022) **DOI:10.1007/s00158-022-03343-5**.

[32] Liu, W., Wu, C., Chen, X. An eigenfrequency-constrained topology optimization method with design variable reduction. *Stroj Vestn-J Mech E* 70 159-169 (2024) **DOI:10.5545/sv-jme.2023.739**.

[33] Yu, Y., Song, Y., Zhao, L., Zhao, C. Analytical formulae and applications of vertical dynamic responses for railway vehicles. *Stroj Vestn-J Mech E* 69 73-81 (2023) **DOI:10.5545/sv-jme.2022.375**.

[34] EN 12663:2010. *Railway applications - Structural requirements of railway vehicle bodies - Part 1: Locomotives and passenger rolling stock (and alternative method for freight wagons).* (2010) European Committee for Standards, Brussels.

[35] Hsu, Y.L. A review of structural shape optimization. *Comput Ind* 25 3-13 (1994) **DOI:10.1016/0166-3615(94)90028-0**.

[36] Falconi, D.C.J., Walser, A.F., Singh, H., Schumacher, A. Automatic generation, validation and correlation of the submodels for the use in the optimization of crashworthy structures. Schumacher, A., Vietor, T., Fiebig, S., Bletzinger, KU., Maute, K. (eds.) *Advances in Structural and Multidisciplinary Optimization: Proceedings of the 12th World Congress of Structural and Multidisciplinary Optimization* 1558-1571 Springer, Cham (2018) **DOI:10.1007/978-3-319-67988-4_117**.

[37] Ozturk, U.E. Efficient method for fatigue based shape optimization of the oil sump carrying a differential case in four wheel drive vehicles. *Struct Multidisc Optim* 44 823-830 (2011) **DOI:10.1007/s00158-011-0678-z**.

[38] Sracic, M.W., Elke, W.J. Effect of boundary conditions on finite element submodeling. *Nonlinear Dynam* 1 163-170 (2019) **DOI:10.1007/978-3-319-74280-9_16**.

[39] Tanino, T. Sensitivity analysis in multiobjective optimization. *J Optim Theory Appl* 56 479-499 (1988) **DOI:10.1007/BF00939554**.

[40] Ranjbar, H., Ahmadi, H. Sheshdeh, R.K., Ranjbar, H. Application of relative sensitivity function in parametric optimization of a tri-ethylene glycol dehydration plant. *J Nat Gas Sci Eng* 25 39-45 (2015) **DOI:10.1016/j.jngse.2015.04.028**.

Declaration of Competing Interest *The authors declare that they have no known competing financial interests or personal relationships that could have appeared to influence the work reported in this paper.*

Acknowledgements *The Science and Technology Project Plan of Transportation Department of Liaoning Province (202246), the Fundamental Research Funds for the Provincial Universities of Liaoning (LJ212410150009) and the paper is supported by the Foundation of Liao Ning Educational Department (LJKMZ20220842). The author would like to express his gratitude to its support to this research.*

Received 2025-03-04, revised 2025-08-03, accepted 2025-09-11
as Original Scientific Paper 1.01.

Data Availability *The data supporting the findings of this study are included in the article.*

Author Contribution *Delei Du: Formal analysis, Funding acquisition, Project administration, Writing-original draft, Writing-review & editing. Yana Li: Writing-review & editing. Jian Song: Methodology, Writing-review & editing. Zhengping He: Writing-review & editing. Data curation, Resources, Writing-review & editing. Jianxin Xu: Conceptualization, Methodology, Writing-review & editing.*

Dvostopenjska optimizacija zasnove spodnjega okvirja metroja na osnovi metodologije hkratne optimizacije topologije, velikosti in oblike

Povzetek *Zasnova konstrukcije karoserije metroja mora zadoščati uravnoteženju varnostnih in stroškovnih kazalnikov. Spodnji okvir ni le glavni nosilni element karoserije metroja, temveč predstavlja tudi pomemben delež njene skupne mase. Ta članek se osredotoča na zmanjšanje obratovalnih stroškov in izboljšanje varnostne zmogljivosti karoserije metroja z optimizacijo zasnove spodnjega okvirja. Predlagan je bil dvostopenjski pristop k optimizaciji, ki nadgrajuje omejitve obstoječih metod in obravnava izzive pri uravnoteženju realnih obratovalnih pogojev s tehnologičnostjo. Najprej so bile v postopek vključene proizvodne omejitve z uporabo metode spremenljive gostote, pri čemer je bila izvedena topološka optimizacija delnega modela spodnjega okvirja z namenom minimizacije deformacijske energije, utežene glede na prožnost. Nato je bila groba topologija izboljšana s parametrično optimizacijo po določitvi približne oblike prereza, kar je privedlo do natančnejšega modela. Rezultati kažejo, da predlagana metoda optimizacije zmanjša maso spodnjega okvirja za približno 4,7 %, hkrati pa zmanjša največji upogibek karoserije metroja pri maksimalni navpični obremenitvi za 0,601 mm. To dokazuje, da predlagana metodologija učinkovito združuje optimizacijske zmogljivosti in preprostost.*

Ključne besede *spodnji okvir metroja, optimizacija strukture, kooperativna optimizacija, zmanjšanje mase*